PNAS RESEARCH ARTICLE | NEUROSCIENCE

A synaptic filtering mechanism in visual threat identification in mouse

Qiwen Wu[a,b], E. Li[a,1], and Yifeng Zhang[a,2]

Edited by Winfried Denk, Max-Planck-Institut fur biologische Intelligenz Campus Martinsried, Martinsried, Germany; received July 26, 2022; accepted November 17, 2022

Predator detection is key to animal's survival. Superior colliculus (SC) orchestrates the animal's innate defensive responses to visually detected threats, but how threat information is transmitted from the retina to SC is unknown. We discovered that narrow-field neurons in SC were key in this pathway. Using in vivo calcium imaging and optogenetics-assisted interrogation of circuit and synaptic connections, we found that the visual responses of narrow-field neurons were correlated with the animal's defensive behaviors toward visual stimuli. Activation of these neurons triggered defensive behaviors, and ablation of them impaired the animals' defensive responses to looming stimuli. They receive monosynaptic inputs from looming-sensitive OFF-transient alpha retinal ganglion cells, and the synaptic transmission has a unique band-pass feature that helps to shape their stimulus selectivity. Our results describe a cell-type specific retinotectal connection for visual threat detection, and a coding mechanism based on synaptic filtering.

retinotectal connection | SC | looming | band-pass filtering | innate defensive behaviors

Significance

The presence of a fast-incoming predator needs to be identified immediately as a danger, so proper defensive behaviors can be initiated. Meanwhile, false alarms should be avoided to preserve energy. How visual threat signal is identified during the transmission from the eye to the brain is unknown. This report identified a cell-type specific connection from the retina to the superior colliculus that was likely central to identifying visual threats and initiating escape. It also studied the transmission of visual information in this connection and revealed a band-pass filtering with millisecond precision. Such precise filtering has rarely been observed in the nervous system before. This band-pass filtering helps the brain to better distinguish visual threats from other visual inputs.

Predator-like looming stimuli reliably evoke defensive behaviors in many species, including humans (1–6). In mice, this stimulus effectively triggers defensive behaviors, such as escape and freezing (7). The detection of visual threats starts in the retina, with multiple types of retinal ganglion cells (RGCs) implicated in the process, including OFF-transient alpha retinal ganglion cells (OFFt αRGCs) (8–11). The information is then sent to the superior colliculus (SC) which is a key hub in processing visual threats and initiating the innate defensive behaviors (12–17). The superficial part of SC (sSC) receives retina inputs topographically (18). There are at least four morphologically identified cell types within sSC, with distinct functions: wide-field cells, narrow-field cells, stellate cells, and horizontal cells (19, 20). Gene expression profiling suggests that there are more types yet to be described (21). Parvalbumin (PV) expressing sSC neurons are implicated in the innate defensive behaviors triggered by visual threats (12, 14). But PV^+ neurons partially overlap with multiple neuronal types including the four mentioned above (14, 22), which specific type or types of sSC neurons mediate these responses is not yet clear. More importantly, how visual threat information is transmitted from the retina to the sSC, and how this signal transmission process impacts the behavioral responses remain largely unknown.

Synapses are fundamental processing units of the brain. The effect of signal transmission between individual neurons varies dramatically, depending on passive membrane properties and active synaptic plasticity (23, 24). Short-term synaptic plasticity, occurring from millisecond to minutes, enables activity history-based computation in the synapse. Such spike timing-related encoding has been implemented in multiple brain functions, including sensory processing (25, 26), and it greatly increases the computational capacity of neurons (27). With short-term plasticity, synapses may serve as temporal filters, transmitting spikes with different efficiency based on the preceding inter-spike intervals (ISIs) (28, 29). However, research connecting synaptic filtering to specific physiological functions of the neural system is still scarce.

Here, we studied the visual responses of a functionally and morphologically uniform neuronal population in the sSC, the Grp^+ narrow-field neurons, and showed that they had the same selectivity as visually evoked defensive behaviors. The role of Grp^+ neurons in visually triggered innate defensive behaviors was then tested with optogenetic activation and cell ablation experiments. Grp^+ neurons receive inputs from OFFt αRGCs, which mediate the looming evoked defensive responses in the retina. Interestingly, we found that the connections between the Grp^+ neurons and OFFt αRGCs were narrowly band-passed, so that only spikes spaced 9 ms apart could pass through effectively. This band-pass filtering contributes to the selective defensive responses of the mice to visual threats, but not to other innocuous visual inputs.

Author contributions: Q.W. and Y.Z. designed research; Q.W. and E.L. performed research; Q.W., E.L., and Y.Z. analyzed data; and Q.W. and Y.Z. wrote the paper.

The authors declare no competing interest.

This article is a PNAS Direct Submission.

Copyright © 2022 the Author(s). Published by PNAS. This article is distributed under Creative Commons Attribution-NonCommercial-NoDerivatives License 4.0 (CC BY-NC-ND).

[1]Present address: Xiangtan Medicine and Health Vocational College, Xiangtan, Hunan 411104, China.

[2]To whom correspondence may be addressed. Email: zh.yifeng@gmail.com.

This article contains supporting information online at https://www.pnas.org/lookup/suppl/doi:10.1073/pnas.2212786120/-/DCSupplemental.

Published December 27, 2022.

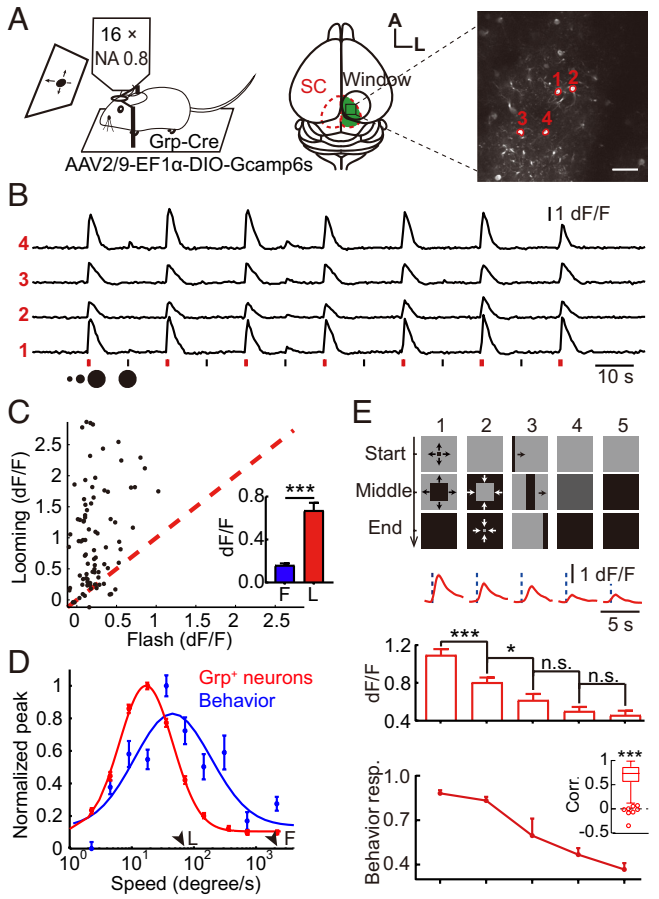

Fig. 1. Grp$^+$ neurons selectively respond to the looming stimulus. *A*, Schematic diagram of in vivo calcium imaging in amSC. *Right*, an example image, numbers indicate four Grp$^+$ neurons whose calcium signals are shown in *B*. (Scale bar, 50 μm.) *B*, Calcium responses of four Grp$^+$ neurons to repeated looming (L) and flash (F) stimuli. *C*, Comparison of Grp$^+$ neurons' response to looming and flash. Each point represents one recorded neuron. *Inset*, comparison of averaged calcium responses. N = 87 cells in four mice, 7 to 10 repeats each. Error bars, SEM. Paired *t* test, *P**** < 0.001. *D*, Looming speed tunings of the Grp$^+$ neurons (red) and the behavior response (blue) with Gaussian fits. Error bars, SEM. Behavior, N = 16 to 63 trials from 8 to 30 mice for different data points; Grp, N = 90 cells in four mice. Arrowheads, the speeds of looming (L) and flash (F) used in *B*. *E*, The responses of Grp$^+$ neurons to different visual stimuli match the behavior responses of the mice. *Top*, visual stimuli. *Middle*, calcium responses of a Grp$^+$ neuron (raw trace) and average responses of all Grp$^+$ neurons (bar plot). Error bars, SEM. *Bottom*, corresponding behavior responses, as measured by the response latency index (25 − latency)/25, where 25 s is the duration of the stimulus, and the cutoff latency for mice that did not respond. *Inset*, correlation between the calcium responses of the Grp$^+$ neurons and the behavior responses of the mice to the same types of visual stimuli. Line, median; boundaries of the box, upper and lower quartiles; whiskers, maxima and minima; individual points, outliers. N = 91 neurons in four mice for calcium responses. N = 40/8/9/21/30 mice for the five stimuli, respectively, 1 to 3 trials per mouse. Paired *t* test for calcium responses, *P**** < 0.001, *P** < 0.05, n.s., not significant. One sample *t* test for correlation coefficient, *P**** < 0.001.

Results

The Visual Responses of SC Narrow-Field Neurons Showed the Same Selectivity of Visually Triggered Innate Defensive Behaviors. Narrow-field neurons in the sSC can be specifically labeled by a Grp-Cre transgenic line (19). The soma of adeno-associated virus (AAV)-labeled Grp$^+$ neurons were restricted to a lamina at the intermediate depth of sSC, and the neurons showed distinct morphology consistent with that of the narrow-field neurons (*SI Appendix*, Fig. S1*A*) (19). We first investigated the visual responses of the sSC neurons labeled by this line (Grp$^+$ neurons) in head-fixed two-photon calcium imaging using GCaMP6s (Fig. 1*A*). Since threats to mice typically come from above, the visual stimuli were presented from a front overhead monitor. Retinotopically matching the stimulus location, the imaging site was at the anteromedial SC (amSC). Grp$^+$ neurons responded strongly toward a gradually enlarging dark disk (looming stimulus), but only minimally to the sudden appearance of the same dark disk (flash stimulus) (Fig. 1 *A*–*C* and Video S1). We also tested the behavior responses of mice toward the same stimuli. Two parameters were used to measure the behavior responses: escape speed and response latency. The stronger the behavior response, the faster the escape speed, and the shorter the response latency. Mice responded to looming with innate defensive behaviors but were mostly indifferent to a flash stimulus (Fig. 1*D*). The same selective response to looming but not flash has also been observed in zebrafish (30). Closer examination revealed that the responses of the Grp$^+$ neurons to a looming object depended on the speed of the expanding motion with a bell-shaped tuning, and the behavioral responses of the mice followed a similar trend (Fig. 1*D*). Furthermore, we tested the responses of the Grp$^+$ neurons to other types of visual stimuli, as well as the behavioral responses of the mice toward these stimuli. A clear match between the behavior responses and the calcium responses of Grp$^+$ neurons was observed (Fig. 1*E* and *SI Appendix*, Fig. S1*B*). For comparison, we recorded the responses of random neurons in the sSC, and Vgat$^+$ neurons, which are Grp-negative inhibitory neurons (*SI Appendix*, Fig. S1 *C* and *D*). The responses were much more varied, with sometimes opposite calcium responses in different neurons. They were also not as tightly correlated with defensive behaviors as the responses of Grp$^+$ neurons (*SI Appendix*, Fig. S1*E*). Thus, this matching of selectivity between innate defensive behaviors and neuronal activities appeared to be specific to the Grp$^+$ neurons.

Activation of Grp$^+$ Neurons Induced Defensive Behaviors. We tested the effects of optogenetic activation of Grp$^+$ neurons (Fig. 2*A*). ChR2 was specifically expressed in Grp$^+$ neurons in amSC (*SI Appendix*, Fig. S2*A*) and activated by light pulses at 20 Hz with a pulse duration of 20 ms. Dramatic increase in motion speed was observed immediately after the light onset (Fig. 2 *B* and *C*), followed by the mouse entering the shelter and staying immobile for a prolonged time (Fig. 2*B* and Videos S2 and S3). Actually, a single 20-ms pulse of laser was already able to induce fast escape in many mice (*SI Appendix*, Fig. S2 *B* and *C* and Video S4). This sequence of behavior is the same as mice responding to a looming object (7). Activation of GRPR$^+$ or SST$^+$ neurons in the sSC did not trigger similar responses (*SI Appendix*, Fig. S2 *D* and *E*) (12), suggesting that this is a cell-type-dependent phenomenon. We also tested whether different levels of activation in Grp$^+$ neurons produced different behavioral consequences. Weaker activation, such as shortening the pulse duration from 20 ms to 2 ms, induced fewer spikes in Grp$^+$ neurons (Fig. 2 *D* and *E* and *SI Appendix*, Fig. S2*F*) and slower escapes with longer latencies in mice (Fig. 2 *F* and G and Video S5). For all mice tested, reducing the stimulus strength further switched the response from escape to freezing (Fig. 2*H* and Video S6). Thus, moderate-to-strong activation of Grp$^+$ neurons triggered a "dose-dependent" escape response, while weak activation induced freezing.

Mice respond to overhead looming object with robust defensive responses but are generally indifferent if the same looming stimulus is presented from side or below (7, 17). If Grp$^+$ neurons are important for such visually induced innate defensive responses, we may observe the same dependency on spatial location in Grp$^+$ neuron-mediated defensive responses. According to the retinotopic map of SC (31), overhead visual stimuli are processed by amSC, whereas visual stimuli from behind and below are processed by posterolateral SC (plSC). We therefore compared the effects of

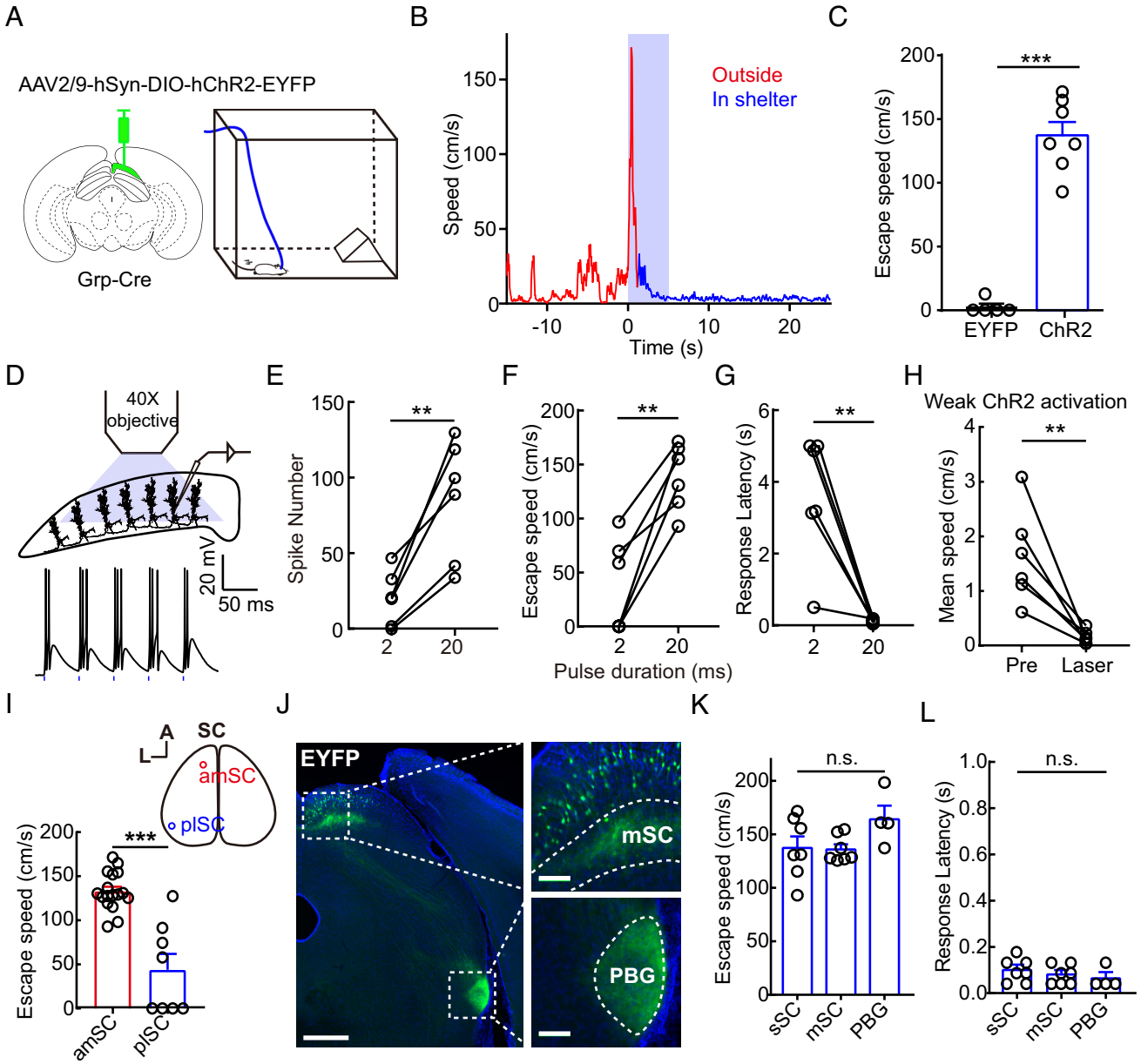

Fig. 2. Activation of Grp$^+$ neurons elicited defensive behaviors. *A*, Diagram of optogenetic activation of Grp$^+$ neurons in amSC. *B*, A representative response to the activation of Grp$^+$ neurons. Motion speed of the mouse through time is plotted, with color indicating the location of the mouse. Blue shaded area, 5 s of 470-nm laser pulses at 20 Hz, 20 ms pulse duration. *C*, Comparison of peak escape speeds from the control (EYFP) and Grp$^+$ activation (ChR2) groups. EYFP, five mice; ChR2, seven mice. Unpaired *t* test. *D*, Representative current clamp recordings of Grp$^+$ neurons during optogenetic activation. *Upper*: experimental setup. *Lower*, light evoked spikes with 2 ms, 20 Hz stimulation. Blue dots, light stimuli. *E*, Average numbers of spikes induced by 20 light pulses at 20 Hz, with 2 ms and 20 ms pulse duration. N = 6 cells in two mice. Paired *t* test. *F* and *G*, Comparison of peak escape speed (*F*) and response latency (*G*) between 20 Hz activations using 2 ms and 20 ms pulse durations. N = 6 mice. Paired *t* test. *H*, Mean speed of mice 5 s before and during weak optogenetic activation (see *Methods*) of Grp$^+$ neurons. N = 6 mice. Paired *t* test. *I*, Comparison of peak escape speed between amSC and plSC activation. amSC, 17 mice; plSC, 8 mice. *Upper Right*, relative positions of amSC and plSC. Unpaired *t* test. *J*, Projection pattern of Grp$^+$ neurons revealed by sSC injection of AAV2/9-hEF1α-DIO-EYFP in a Grp-Cre mouse. Axon terminals are mainly enriched in mSC (*Upper Inset*) and PBG (*Lower Inset*). [Scale bars, 500 μm (*Main*) and 100 μm (*Insets*)]. *K* and *L*, Comparison of peak escape speed (*K*) and response latency (*L*) between somatic activation of Grp$^+$ neurons in the sSC (seven mice) and axon terminal activations in the mSC (seven mice) or PBG (four mice). One-way ANOVA. *P**** < 0.001, *P*** < 0.01, n.s., not significant.

Grp$^+$ neuron activation at these two locations. Activation of Grp$^+$ neurons in the amSC induced fast escapes, while activation in the plSC induced much slower escapes (Fig. 2*I*). Thus, Grp$^+$ neurons in amSC are more efficient in mediating escape response than those in plSC, this is consistent with Grp$^+$ neurons being part of the SC circuit for visual threat processing.

Grp$^+$ neurons project to both the parabigeminal nucleus (PBG) and the intermediate SC (mSC) (Fig. 2*J*) (19). We tested the behavior outcome of separately activating these two axon branches. The tip of the optic fiber was placed in either superficial SC to activate the somas, or in mSC or PBG to activate the axonal arbors. No difference in either response latency or escape speed was observed (Fig. 2 *K* and *L*). Due to the close proximity of mSC and sSC, separate activation of sSC somas and mSC axon terminals of the Grp$^+$ neurons may not be achievable by this method. Nevertheless, at least for activation of Grp$^+$ neurons' axon projections in PBG, the behavior responses appeared to be the same as soma activation. Also similar to soma activation, weak activation of the Grp$^+$ neurons' terminals in PBG induced freezing behavior (*SI Appendix*, Fig. S2*G*). Moreover, activation of Vglut2$^+$, but not Rorb$^+$ or ChAT$^+$ neurons

in PBG, elicited rapid escape behavior (*SI Appendix*, Fig. S2 *H* and *I*) (14), whereas weaker activation of the same population of neurons induced freezing instead (*SI Appendix*, Fig. S2*J*), much the same as the activation of Grp$^+$ neurons in sSC.

Together, these results suggested that activation of Grp$^+$ neurons elicited defensive behaviors through their connections to the Vglut2$^+$ neurons in PBG and highlighted the importance of SC narrow-field neurons in the innate defensive responses. Further, Grp$^+$ neurons are uniform in morphology, function, and connection (*SI Appendix*, Fig. S1*A*) (19), but can induce escape or freezing responses under different activation paradigms, thus they may be the neurons where the choice between escape and freezing is initially made.

Ablation of Grp$^+$ Neurons Impaired the Defensive Behaviors. We next ablated Grp$^+$ neurons using AAV-mediated expression of Caspase3, then examined the animal's defensive responses to visual threats (Fig. 3*A*). More than 75% of Grp$^+$ cells in the amSC were ablated in the ablation group (Fig. 3 *B* and *C*). Afterwards, their behavior responses to overhead looming stimuli were analyzed and compared to mice that expressed EYFP instead of Caspase3 in the Grp$^+$ neurons. Under the same testing condition (*SI Appendix*, Fig. S3 *A* and *B*), the ablation group responded to the looming stimulus with higher probability of freezing and slower escapes (Fig. 3 *D*–*G*, *SI Appendix*, Fig. S3*C*, and Videos S7–S9). Freezing is a response to milder visual threats compared to fleeing (32).

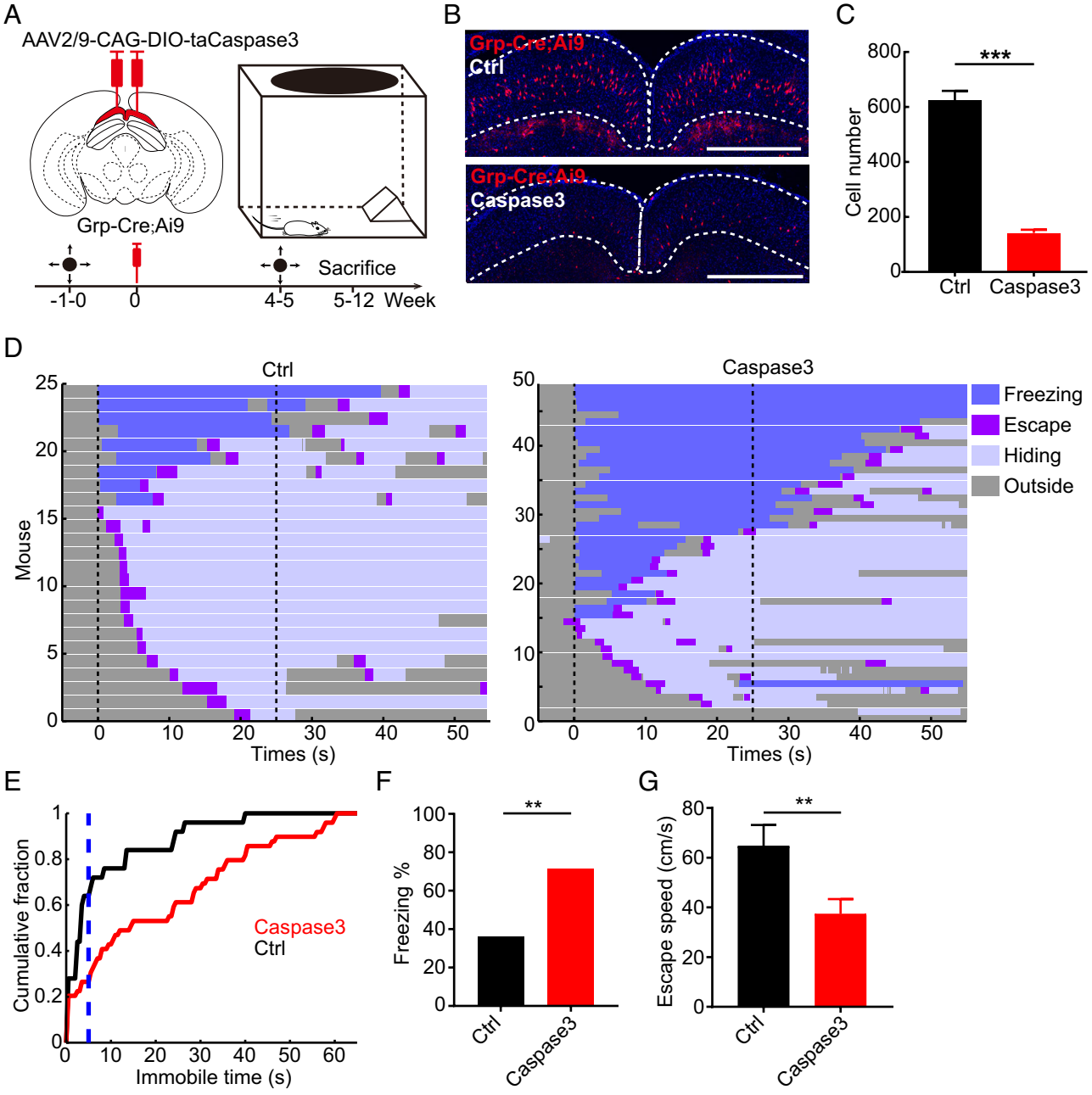

Fig. 3. Grp$^+$ neurons participate in looming evoked defensive behaviors. *A*, Diagram of the Grp$^+$ neuron ablation experiment. *B*, Example of GrpAi9 expression in control and Caspase3 group. (Scale bar, 500 μm.) *C*, Numbers of Grp$^+$ cells in amSC, in the control and Caspase3 groups. Control, 8 mice; Caspase3, 37 mice. Unpaired *t* test. *D*, Behavior responses of individual mice to looming in the control (*Left*) and Caspase3 (*Right*, ablation) groups. Black dashed lines, the onset and offset of the looming stimulus. *E*, Cumulative distributions of immobile time in looming responses. Blue: threshold for freezing. *F* and *G*, Comparison of freezing probability (*F*) and peak escape speed (*G*) between the control and the ablation groups. *F*, Fisher's exact test; *G*, unpaired *t* test. *P**** < 0.001, *P*** < 0.01. N = 25/49 for control/Caspase3, in *D*–*G*.

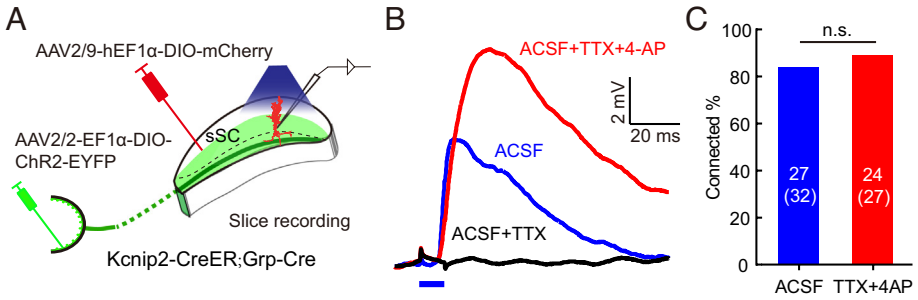

Fig. 4. Grp$^+$ neurons receive monosynaptic inputs from OFFt αRGCs. *A*, Schematic diagram for testing the connections between OFFt αRGCs and the Grp$^+$ neurons. *B*, Representative response of a Grp$^+$ neuron to terminal activation of OFFt αRGCs, in artificial cerebrospinal fluid (ACSF, blue), during TTX (black) and together with 4-AP (red) perfusion. Short blue line, optogenetic stimulation. Mean of five trials. *C*, The fractions of recorded Grp$^+$ neurons with inputs from OFFt αRGCs. Fisher's exact test, n.s., not significant.

And as shown above, weaker activation of Grp$^+$ neurons induced freezing instead of fleeing (Fig. 2*H*). Thus, the transition from fleeing to freezing reflects the attenuation of behavioral response after the ablation of Grp$^+$ neurons. These results suggest that one, Grp$^+$ neurons are involved in the SC circuit for visual threat responses, and two, Grp-Cre likely only partially labels the SC neurons in this pathway, since the responses to looming were merely attenuated when most Grp$^+$ neurons were ablated. These results are also consistent with Grp$^+$ neurons being involved in the choice between freezing and escape behaviors.

Grp$^+$ Neurons Receive Band-Pass Filtered Inputs from OFFt αRGCs. OFFt αRGCs are a type of RGCs critical for transmitting visual threat signals from the retina to the SC, and they can be labeled by Kcnip2-CreER with more than 90% accuracy (8, 33). If Grp$^+$ neurons are indeed a key component of the SC circuit that processes the visual threat signals, we expect them to receive inputs from the OFFt αRGCs. We expressed ChR2 in OFFt αRGCs and mCherry in Grp$^+$ neurons (*SI Appendix*, Fig. S4*A*). Using the SC slice preparations, axon terminals of the OFFt αRGCs were optogenetically activated, and the postsynaptic potentials (PSPs) were recorded in the fluorescently labeled Grp$^+$ neurons (Fig. 4*A*). PSPs with short latencies were observed in more than 80% of recorded Grp$^+$ neurons (Fig. 4 *B* and *C* and *SI Appendix*, Fig. S4*B*). Considering the limited efficiency of viral infection of the OFFt αRGCs, this was likely an underestimate of the actual connection probability between the OFFt αRGCs and the Grp$^+$ neurons. Tetrodotoxin (TTX) was then used to suppress action potentials to isolate monosynaptic responses, and 4-aminopyridine (4-AP) was perfused at the same time to block voltage-dependent potassium channels to enhance presynaptic responses. A similar probability of connection was observed in the presence of TTX and 4-AP (Fig. 4 *B* and *C* and *SI Appendix*, Fig. S4*C*), indicating that almost all Grp$^+$ neurons form monosynaptic connections with OFFt αRGCs. This ratio of connection to the OFFt αRGCs was significantly higher than observed in the GAD67$^+$ neurons or randomly selected SC neurons whose somas were in the vicinity of Grp$^+$ neurons (*SI Appendix*, Fig. S4*D*).

Are Grp$^+$ neurons' visual responses mostly inherited from OFFt αRGCs? We recorded the responses of OFFt αRGCs to looming and flash stimuli. Their peak response to flash was significantly higher than to looming (*SI Appendix*, Fig. S5 *A* and *B*). Thus, the synaptic transmission between the OFFt αRGCs and Grp$^+$ neurons must convert the stronger OFFt αRGC input in response to flash to a weaker output in the Grp$^+$ neurons, and a weaker input after looming to a stronger output. How is this conversion achieved? Closer examination revealed that despite the difference in peak firing rates, the total number of spikes elicited by flash was roughly the same as by looming (*SI Appendix*, Fig. S5*B*). The difference between the two responses thus lies mostly in the temporal structure. Flash response had a peak ISI distribution at 4 to 5 ms, whereas looming responses peaked at 6 to 10 ms (*SI Appendix*, Fig. S5*C*). Compared to flash, looming responses had an excess of ISI distributions at 6 to 15 ms (*SI Appendix*, Fig. S5*C*). Thus, a synapse that preferentially transmit action potentials with ISIs at 6 to 15 ms would give preferential response to looming in the downstream neurons.

We examined how synaptic transmission between OFFt αRGCs and the Grp$^+$ neurons was affected by the ISIs. Paired light pulses with different inter-pulse intervals (IPIs) were used to stimulate the axon terminals of OFFt αRGCs, and the PSPs were recorded from Grp$^+$ neurons in SC slices (Fig. 5 *A* and *B*). Paired-pulse ratios (PPRs) were then measured for different IPIs. In addition to a low-pass component for IPIs larger than 30 ms, there was also a band-pass component in this transmission (Fig. 5*C*). The passband was centered at roughly 9 ms with a width of 4 to 5 ms (Fig. 5*D*), matching the range of ISIs enriched in the looming responses (*SI Appendix*, Fig. S5*C*).

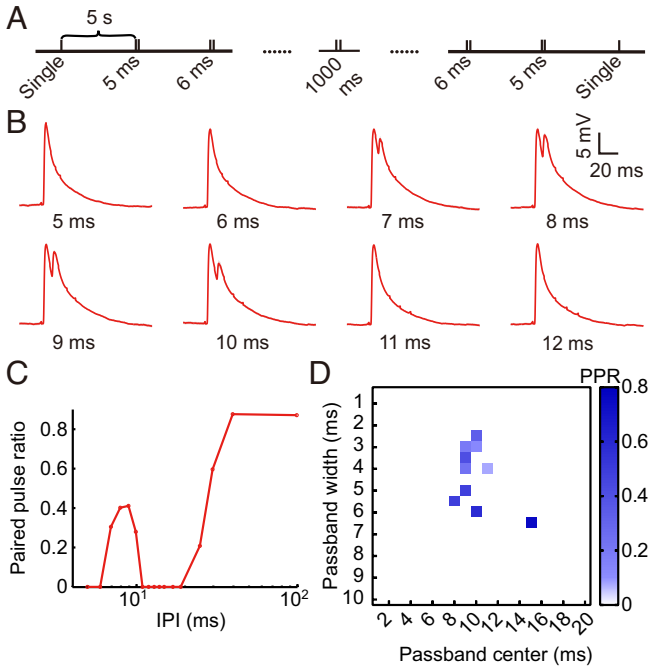

Fig. 5. Grp$^+$ neurons form band-pass synapses with OFFt αRGCs. *A*, Stimulus design for testing the synaptic transmission from OFFt αRGCs to the Grp$^+$ neurons. Each pulse was a flash (1 to 2 ms) of 470-nm light. *B*, Response of a Grp$^+$ neuron to paired optogenetic pulses. Mean PSPs from 20 trials. Light red area, SEM. IPIs are indicated below each trace. *C*, A representative PPR plot. *D*, Summary of the passband properties. N = 10 neurons from five mice.

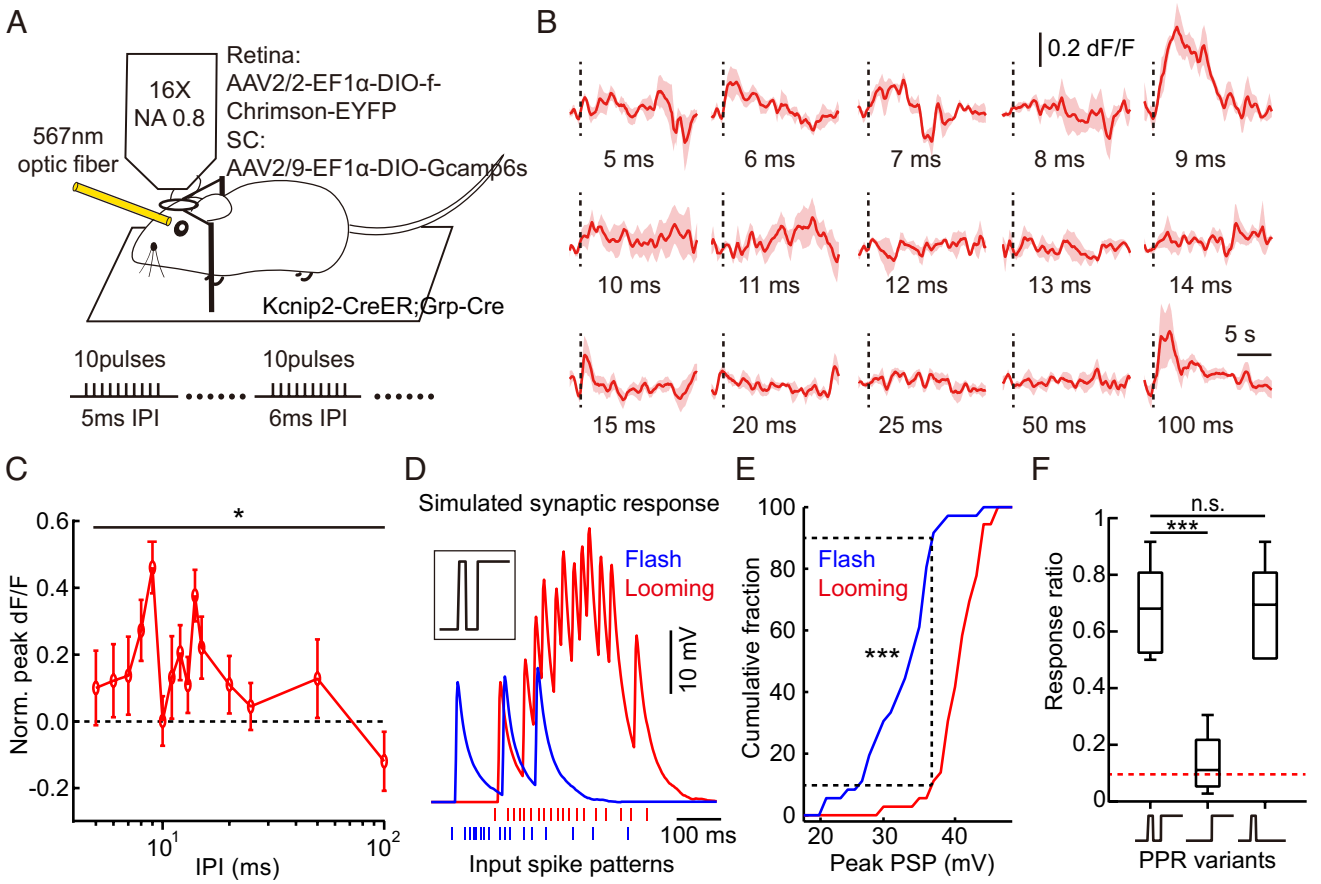

Fig. 6. Band-pass synaptic transmission underlies the selectivity of Grp$^+$ neurons. *A*, Experimental design for testing the synaptic transmission between OFFt αRGCs and Grp$^+$ neurons in vivo in awake mice in amSC. *B*, Calcium responses of a Grp$^+$ neuron after optogenetic activation of OFFt αRGCs using pulses with different IPIs in awake mice. N = 4 trials, light red area, SEM. *C*, Average calcium responses of Grp$^+$ neurons to OFFt αRGCs activation with different IPIs in awake mice. N = 22 cells, five imaging areas, two mice. One-way ANOVA, *P** < 0.05. *D*, Simulated responses of a Grp$^+$ neuron with inputs from OFFt αRGCs. *Inset*, PPR used for simulation; *Bottom*, input spike trains. *E*, Cumulative distribution of peak amplitudes of simulated PSPs using input spike trains from a representative OFFt αRGC. Dashed lines: vertical, response threshold; upper/lower, response ratios for flash/looming, respectively. One-way ANOVA with Holm–Sidak's post hoc test. *F*, Stimulus selectivity of simulated responses differ with different PPR variants (*Bottom*). *P**** < 0.001, *P*** < 0.01, *P** < 0.05, n.s., not significant.

We next asked whether the synapses behaved in a similar fashion in vivo (Fig. 6*A*). AAV-mediated expression of f-Chrimson was used to control the activity of OFFt αRGCs with high temporal precision (34). Photoreceptors were removed pharmacologically so that the retinal inputs to the Grp$^+$ neurons were solely from f-Chrimson-mediated activation of OFFt αRGCs (35). To prevent possible interference from intrinsically photosensitive RGCs (ipRGCs), we designed the optogenetic stimuli to have the same total light flux, so that ipRGCs would respond indistinguishably to all stimuli (36). OFFt αRGCs were activated by trains of light pulses with different IPIs, producing spike trains with dominant ISIs matching the IPIs (*SI Appendix*, Fig. S6), while the calcium responses of Grp$^+$ neurons were recorded (Fig. 6 *B* and *C*). The responses peaked when the stimulus IPIs were at 8 to 9 ms, corroborating the band-pass transmission (Fig. 5 *B* and *C*). The lower but wider peak around 14 ms IPI may be explained by the intervals between the second spike from a light pulse and the first spike from the next pulse falling within this 8 to 9 ms range (*SI Appendix*, Fig. S6 *B* and *C*). Moreover, the low-pass component in the PPR curve was missing in these calcium responses, likely because the synaptic responses from single pulses were hardly summed when IPIs exceeded 30 ms. Effectively, the signal transmission from the OFFt αRGCs to the Grp$^+$ neurons was band-passed.

The Band-Pass Transmission Underlay the Preferential Response to Looming. Since Grp$^+$ neurons may receive inputs from multiple types of RGCs, we examined if the inputs from OFFt αRGCs alone, coupled with the band-pass transmission, were sufficient to produce the observed selective response to looming but not flash. With spiking responses of recorded OFFt αRGCs and a simplified synaptic transmission mimicking the recorded ones, we simulated the membrane potential changes in the Grp$^+$ neurons under either a looming or a flash stimulus (Fig. 6*D*). The simulated depolarization from looming was significantly larger than from flash (Fig. 6 *D* and *E*). With a response threshold that allowed 10% of flash trials to respond, nearly 75% of looming trials responded, resonating the significant advantage of looming over flash in inducing responses in Grp$^+$ neurons and defensive behaviors in animals (Fig. 1*D*). Since the PPR curve had two distinct components, a band-pass one at ~9 ms, and a low-pass one with the cutoff at ~30 ms, we tested them separately in simulation. The band-pass filter alone was sufficient to achieve roughly the same performance in selecting looming over flash, whereas the low-pass part was not able to separate the two stimuli (Fig. 6*F*). Thus, with sole inputs from OFFt αRGCs and band-pass synaptic transmission, Grp$^+$ neurons are capable of preferentially responding to looming stimulus, despite the higher peak firing rate of OFFt αRGCs under flash stimulus, illustrating an interesting coding strategy based on synaptic filtering.

Discussion

In this report, we found that Grp$^+$ neurons in the superficial SC selectively responded to looming stimuli and were critical for

innate defensive behaviors induced by visual threats. The Grp^+ neurons form narrowly band-passed synapses with upstream looming sensitive OFFt αRGCs, and this band-pass filtering allows the transmission of looming signals, but not flash signals from the OFFt αRGCs. Such a visual coding strategy based on band-pass filtering with millisecond precision is rarely seen. Although trans-synaptic tracing methods have been successfully employed before to map connections between the retina and the SC (37, 38), the current report functionally described such a retinotectal connection in a cell-type specific manner. Band-pass synaptic transmission has been observed before in fish (39) and mammals (23, 40), but with much wider bandwidth, more variable passband locations and significantly weaker selectivity. These earlier data were from mixed neuronal populations. In contrast, our results benefited from the use of a cell-type specific system, where both the presynaptic and postsynaptic neurons are cleanly defined by transgenic lines and are morphologically and functionally uniform (8, 19). Between OFFt αRGCs and the Grp^+ neurons, the band-pass synaptic transmission had millisecond precision: a couple of milliseconds' difference in ISI could result in a difference in PPR between 0 and as much as 0.8. Such precise band-pass filtering can improve the efficacy of synaptic computation and may not be unique to this specific synapse. Furthermore, the ISI distributions for flash and looming vary under different illumination conditions. Thus, to always respond selectively to looming in different visual environments, the passband location may need to be modulated constantly. The mechanisms underlying the formation and modulation of this unique band-pass transmission deserve further investigation. It's also worth noting that the band-pass filtering cannot explain all the differences in stimulus selectivity between the OFFt αRGCs and the Grp^+ neurons. For example, OFFt αRGCs respond to a white contracting disk and a dark expanding disk in much the same way, but Grp^+ neurons only respond to the latter, not the former. Thus, other retinal channels must be involved to distinguish these two stimuli. Isolation and description of these retinal channels will help better understand the process of visual threat identification in SC.

We used two optogenetic proteins, ChR2 (41) and f-Chrimson (34), to activate axon terminals of OFFt αRGCs. The band-pass synaptic transmission was observed in both types of preparations, minimizing the possibility that this was an artifact of the optogenetic proteins. We also directly activated the somas of OFFt αRGCs in the retina and observed that the responses of Grp^+ neurons in vivo were similarly band-pass filtered. However, a significant portion of the optogenetically activated spikes did not follow the intended ISI (*SI Appendix*, Fig. S6 *B* and *C*). Thus, we were unable to activate OFFt αRGCs optogenetically to reproduce their natural looming/flash response patterns. Another caveat of the optogenetic activation experiments is that different OFFt αRGCs were activated simultaneously, whereas they are likely activated sequentially under actual looming stimuli. These problems, regrettably, prevented us from directly observing the responses of the Grp^+ neurons in vivo with sole inputs from OFFt αRGCs with realistic looming/flash spike patterns.

PV^+ neurons in the superficial SC can evoke escape via PBG, and freezing via lateral posterior thalamic nucleus (LP) (14). PV^+ neurons consist of multiple neuronal types, including the narrow-field neurons (22), while the Grp-cre line used in the current report labels only the narrow-field neurons, which project to PBG but not LP (Fig. 2*J*) (19), and was classified by trans-seq to be a single neuronal type (37). It is not clear if the PV^+ neurons mediating the escape behavior are exclusively narrow-field neurons, although our results showed that to be a strong possibility. Meanwhile, LP-projecting PV^+ neurons that mediate freezing need to be further characterized regarding their neuronal-type classification and retinal inputs. Our current result corroborates previous reports on the importance of PBG in generating the escape behavior (12, 14). However, it was also reported that a deep medial SC to dorsal periaqueductal gray (dPAG) pathway was required for escape, and activating this pathway triggered escape even if PBG was inactivated by muscimol (16). This suggests that PBG works either upstream of or in parallel with the dPAG pathway. Grp^+ neurons project to both PBG and mSC (Fig. 2 *J*–*L*), and they may participate in both if the two pathways work in parallel. More research is needed to clarify the relationship between the PBG and the dPAG pathways in the generation of visually guided innate defensive behaviors.

Grp^+ neurons participate in the prey capture behavior (42). And here we showed that they also mediated defensive behaviors. How does the same population of neurons participate in these drastically different behaviors? One possibility is that Grp^+ neurons receiving visual inputs from different parts of the visual field mediate different behaviors, since looming danger likely comes from above whereas small preys are generally on the ground or from the side of the animal. Another possibility is that different firing patterns lead to different behaviors. A looming stimulus and a small moving object signifying a prey are likely detected by different RGCs and may trigger different spiking patterns in the Grp^+ neurons. And we already showed that different activation paradigms of the same Grp^+ neurons could trigger different defensive behaviors. A more comprehensive study on the effects of activity manipulation in the Grp^+ neurons will help to answer these questions.

Methods

Animals. All experiments were performed under the instruction of methods approved by the Animal Care and Use Committee of Center for Excellence in Brain Science and Intelligence Technology, Chinese Academy of Sciences. Mice were group housed (<6 mice/cage) in 12/12-h light and dark cycle. Grp-KH288-Cre (19), Kcnip2-CreER (8), Ai9 (Jackson Lab #007909), SST-Cre (Jackson Lab #013044), GRPR-iCreERT2, Vglut2-Cre (Jackson Lab #016963), Rorb-Cre (Jackson Lab #023526), ChAT-Cre (Jackson Lab #006410), and GAD67-GFP (Jackson Lab #007677) both male and female adult mice (1 to 6 mo old) were used in our study.

Histology. Immunostaining of whole mount retina was performed as described by Wang et al. (8), brain slices were sectioned to 40 to 100 μm routinely. Hoechst (1:10,000, Invitrogen).

Electrophysiology. Retina recording was performed as described by Wang et al. (8). For SC slice recording, mice were anaesthetized with isoflurane and perfused with cold cutting buffer: 92 mM choline, 2.5 mM KCl, 1.2 mM NaH_2PO_4, 30 mM $NaHCO_3$, 20 mM 4-(2-hydroxyethyl)-1-piperazineethanesulfonic acid (HEPES), 25 mM glucose, 5 mM sodium ascorbate, 3 mM sodium pyruvate, 10 mM $MgSO_4$, and 0.5 mM $CaCl_2$. Then 300 μm parasagittal slices were cut with vibratome (DTK-1000N, DOSAKA) and immediately put into warm (34 °C) cutting buffer for 10 min to recover, transferred to holding buffer (92 mM NaCl, 2.5 mM KCl, 1.2 mM NaH_2PO_4, 30 mM $NaHCO_3$, 20 mM HEPES, 25 mM glucose, 5 mM sodium ascorbate, 3 mM sodium pyruvate, 2 mM $MgSO_4$, 2 mM $CaCl_2$, and adjust pH to 7.3 to 7.4 with NaOH) at room temperature for at least 30 min before slice recording in recording buffer (124 mM NaCl, 2.5 mM KCl, 1.2 mM NaH_2PO_4, 24 mM $NaHCO_3$, 5 mM HEPES, 12.5 mM glucose, 2 mM $MgSO_4$, 2 mM $CaCl_2$, and adjust pH to 7.3 to 7.4 with NaOH). TTX (1 μM) and 4-AP (100 μM) was perfused in recording buffer in some preparations. Whole-cell, current-clamp recordings were performed with pipettes filled with potassium internal solution (120 mM K-gluconate, 5 mM NaCl, 10 mM KCl, 1 mM $MgCl_2$, 1 mM ethylene glycol-bis(2-aminoethylether)-N,N,N',N'-tetraacetic acid, 10 mM HEPES, 2 mM adenosine 5'-triphosphate disodium salt, and 0.5 mM guanosine 5'-triphosphate sodium salt hydrate). Electrode resistances were 3 to 9 MΩ. Membrane voltages were acquired with MultiClamp 700B amplifier (Molecular Devices), digitized at 10 kHz, and low-pass filtered at 2 kHz. All the SC neurons were recorded within the lower sSC.

Optogenetic Activation. For slice preparations, optogenetic activation was delivered by light emitting diode (LED), 470 nm for ChR2 or 567 nm for f-Chrimson (Rebel LED, Lumileds), through objective lens with intensity between 1 and 3 mW/mm^2. Pulse duration was typically 1 to 2 ms. First a single pulse activation, then with the IPI sequence [5, 6, 7, 8, 9, 10, 11, 12, 13, 15, 17, 19, 25, 30, 40, 100, 1,000, 100, 40, 30, 25, 19, 17, 15, 13, 12, 11, 10, 9, 8, 7, 6, 5 ms], the sequence was replayed 10 times typically. In the case of retina ex vivo preparations or activation of retina during in vivo imaging, activation was delivered by an optic fiber (Thorlab) from high-power LED (567 nm, Luxeon Star LEDs, 700 mA) with intensity between 9 and 10 mW/mm^2 at the tip. The distance between the tip and the retina was 10 mm (retina explants) or 20 mm (live animals). For in vivo verification of the band-pass filtering, light pulse trains containing ten pulses at a specific IPI were used to test each IPI, pulse duration was 0.1 ms. Intervals between pulse trains were 15 s to ensure full recovery of f-Chrimson. The IPI sequence was [100, 50, 25, 20, 15, 14, 13, 12, 11, 10, 9, 8, 7, 6, 5 ms], replayed 4 to 10 times typically. For behavior experiments, A 473-nm diode pumped solid state laser system (BL47373-050FC, Shanghai Guangteng Company) was used to generate 16-mW laser at the tip of 200-μm optic fiber (FOC-C-W-200-2.5-0.37, Hangzhou Newdoon Technology). For weak activation, stimulation parameters were always weaker (lower frequency and/or shorter pulse duration and/or lower light intensity) than the parameters used to induce fleeing. The power ranged from 1/10 to the same as strong activation with 1 to 2 ms, 10 to 40-Hz light pulses.

Optic Fiber Implantation and Stereotaxic Injection. Mice were anesthetized with 1.5 to 2% isoflurane (R510-22, RWD Life Science) mixed with carbogen using small animal anesthesia machine (Pour Fil R510IP, RWD Life Science), and placed in a stereotaxic frame (Stoelting). Typically, 200 nL AAV constructs at 3 to 10 × 1012 v.g./mL (AAV2/9-hEF1α-DIO-hChR2(H134R)-EYFP-WPRE-pA, AAV2/9-hSyn-GCaMP6s, AAV2/9-hEF1α-DIO-GCaMP6s-WPRE-pA, AAV2/9-hEF1α-DIO-EYFP-WPRE-pA, AAV2/9-hEF1α-DIO-mCherry-WPRE-pA, AAV2/9-CAG-DIO-taCaspase3-TEVp-WPRE-pA, Shanghai Taitool Bioscience Co., Ltd.) were injected into the amSC at coordinates: anteroposterior (AP) −3.52 mm, mediolateral (ML) 0.5 mm, and dorsoventral (DV) −1.40 mm or the plSC (AP −4.24 mm, ML 1.25 mm, and DV −1.40 mm) in (Fig. 2*I*). Injections were done with gastight syringes (10 nL, Hamilton) connected with a pipette at a speed of 20 nL/min, under the control of Motorized Integrated Stereotaxic Injector, Dual (Stoelting). The 200-μm optic fiber was planted into amSC coordinate (AP −3.52 mm, ML 0.5 mm, and DV −1.10 mm), plSC (AP −4.24 mm, ML 1.25 mm, DV −1.25 mm), or PBG (AP −4.24 mm, ML 1.9 mm, DV −3.25 mm). For electrophysiological testing of Kcnip2-Grp connections, AAV2/9-hEF1α-DIO- mCherry-WPRE-pA, AAV2/9-hSyn-DIO-EYFP-WPRE-pA (slice recording), or AAV2/9-hEF1α-DIO-GCaMP6s (in vivo imaging) were injected to the contralateral SC to label Grp$^+$ neurons 2 wk after tamoxifen induction of retinal expressions. For the ablation experiments in Fig. 3, 10 Ai9 mice injected with AAV2/9-CAG-DIO-taCaspase3 and 15 Grp-Cre; Ai9 mice injected with AAV2/9-EF1α-DIO-EYFP were used together in the control group. No difference in behavior was observed between these two groups of control mice.

Intravitreal and Intraperitoneal Injection. For retinal viral injection, mice were anesthetized with avertin (640 mg/kg). Typically, 0.5 μL AAV2/2-EF1α-DIO-ChR2-EYFP or AAV2/2-EF1α-DIO-f-Chrimson-EYFP at 1 × 10^{13} v.g./mL was manually injected intravitreally with a fine glass pipette in the dorsal retina, and 3 to 5 d later, another 0.5 μL virus was injected in the ventral retina to ensure successful expression. 100 μL tamoxifen (ABCONE) (20 mg/mL) was injected intraperitoneally every other day for five times at least 3 d after the second AAV injection. For in vivo optogenetic activation, N-methyl-N-nitrosourea (MNU) (62.5 mg/kg) was injected intraperitoneally at least 1 wk before optogenetic manipulation to remove photoreceptors with minimal impact on other retinal neurons (8, 35). The progressive photoreceptor loss was completed a week after MNU treatment. The experiments were performed soon after to minimize potential compensatory changes in the retinal circuits.

Surgery Preparation and Calcium Imaging. Mice were anesthetized by isoflurane as above, and 3.5-mm-diameter craniotomies were performed on the right hemispheres above the amSC (centered at AP −3.7 mm, ML 1.5 mm). The cortex covering the SC was manually removed carefully. A 3-mm custom-made cranial window, together with a ring-shaped head bar, was glued to the skull with dental cement. Imaging was performed at least 2 wk after surgery. Ketamine (100 mg/kg) and xylazine (10 mg/kg) were administered intraperitoneally prior to calcium imaging. A commercial two-photon microscope (Bruker) was used to image the calcium signals with a 16×, 0.8 NA, 3-mm WD objective (CFI75, Nikon). GCaMP6s was excited with a laser (Mai Tai DeepSee, Spectra Physics) at 920-nm wavelength. Typically, a 494.46 μm × 494.46 μm or 329.64 μm × 329.64 μm field of view was scanned at 1 to 3 Hz as a time series of 512 pixels × 512 pixels.

Behavior Test. All the behavior experiments and related setups were performed in custom-designed sound-attenuating boxes. Mice were put into a custom-made test cage (45 cm L × 45 cm W × 30 cm H) with a shelter (20 cm × 10 cm) at one corner 10 mins before the onset of stimulus. An infrared camera (sampling rate 22 Hz) was used to capture the motion of mice. For visual stimulus test, a computer monitor was put on top of the cage to deliver the stimulus.

Visual Stimuli. For RGC recordings, visual stimuli were projected from a computer-driven Acer K130 projector through a custom lens system onto the retina preparation, with a magnification factor of 8 μm/pixel, and a frame rate of 60 Hz. the stimuli were centered on the receptive field centers of the Kcnip2$^+$ RGCs (OFFt αRGCs). The looming stimulus was a black disc on a gray background, the disc expanded linearly from 0° to 9° (visual angle) within 0.125 s, and held for 2 s. The flash stimulus was the same 9° black disc flashing at 0.5 Hz. For behavioral tests, visual stimuli were displayed on a monitor screen above the test cage. Usually, a black looming disk expanded from 0° to 36° in 0.5 s and then disappeared 1 s later. Ten repeats of the visual stimuli were typically used for each test. For in vivo calcium imaging, visual stimuli were displayed on a small monitor covering 68° of azimuth and 40° of elevation of the left visual field, located 9 cm away from the left eye. Visual stimuli were presented in a 36° × 36° area. Each stimulus condition lasted 5 s to allow slow calcium signals to develop, and each was repeated 5 to 10 times. For visual stimuli in Fig. 1*E*, stimuli 1 and 2 were both expanding disk but with opposite directions of the expanding motion, stimulus 3 was a moving bar, stimulus 4 was gradual dimming, and stimulus 5 was a sudden dark flash.

Simulation. Passband locations were determined from the recorded PPRs by thresholding at 50% of the peak. Binary PPR curves were synthesized based on these passband locations and then used in the simulation. The simulated PSPs were summations of PPR-weighted single PSPs elicited by every spike in the spike train, and the weight (PPR) was determined by the ISI prior to the spike. We set a response threshold such that 10% of the flash trials generated responses, matching the relatively low response probability of Grp$^+$ neurons to flash stimulus, and then used the proportion of looming trials with responses (response ratio) to quantify the selectivity.

Data Analysis. All the data acquired were analyzed using custom codes written in MATLAB (The Mathworks, Natick, MA).

Calcium imaging data: Artifacts of motion were corrected with NoRMCorre (43), segregation of neuronal somas were done manually, and the baseline calcium signals were defined as the calcium signals before stimuli onset. dF/F was computed as the response. All the responses shown in the figures are mean of 5 to 10 repeats. For Fig. 1*E*, the receptive fields of the Grp$^+$ neurons were measured, and only neurons whose receptive fields were within the stimulus area were included. To compare with Vgat$^+$ and random neurons in SC (*SI Appendix*, Fig. S1 *D* and *E*), since many of them did not have receptive field measurements all neurons with measurable responses were included. The correlation between behavior and Grp$^+$ neurons' responses was calculated by the correlation coefficient between the mean behavioral response and normalized calcium response of every neuron. Behavior response was measured by the response latency index: index = (25 − response latency)/25, where 25 s is the duration of the stimulus and the maximal allowable value of latency.

PPR analysis: The amplitudes of the first and second PSP were derived from linearly fitting the recorded PSP trace to the sum of two single PSPs with a time offset matching the given IPIs. PPR was the ratio of the amplitude of the second PSP's amplitude to that of the first PSP. PPRs at different pulse intervals were then plotted to produce the PPR curve shown in Fig. 5*C*. Passband center was determined as the peak location of the passband. Passband width was represented by the full width of the passband at half maximum.

Behavior data: Location of the mice was tracked from 30 s before stimulus onset to 60 s after. Freezing was defined as the period of immobility for longer than 5

s outside of shelter. Escape was defined as the motion that resulted in shelter entrance within stimulation period. The maximum escape speed was defined as the maximum speed (smoothed by sliding average of four frames) of the mice during its escape to the shelter. The response latency was defined as the time between the onset of stimulus to the onset of defensive responses (escape or freezing).

Statistics. All error bars show mean ± SEM. Significance was reported as follows: $P^* < 0.05$, $P^{**} < 0.01$, and $P^{***} < 0.001$. Detailed analysis was defined in figure legends.

Data, Materials, and Software Availability. All study data are included in the article and/or *SI Appendix*.

ACKNOWLEDGMENTS. We thank Prof. Ernst Bamberg for kindly providing the plasmid containing f-Chrimson as a gift. We thank Qingyi Li and Wenting Huang for mice breeding and Xuanzi Cao for technical support. This research was supported by the Recruitment Program of Global Experts, Project supported by Shanghai Municipal Science and Technology Major Project (No. 2018SHZDZX05), and a general project supported by the National Natural Science Foundation of China (No. 31471055).

Author affiliations: [a]Institute of Neuroscience, Center for Excellence in Brain Science and Intelligence Technology, Chinese Academy of Sciences, Shanghai 200031, China; and [b]University of Chinese Academy of Sciences, Beijing 100049, China

1. W. N. Hayes, E. I. Saiff, Visual alarm reactions in turtles. *Anim. Behav.* **15**, 102–106 (1967).
2. T. Preuss, P. E. Osei-Bonsu, S. A. Weiss, C. Wang, D. S. Faber, Neural representation of object approach in a decision-making motor circuit. *J. Neurosci.* **26**, 3454–3464 (2006).
3. K. Yamamoto, M. Nakata, H. Nakagawa, Input and output characteristics of collision avoidance behavior in the frog Rana catesbeiana. *Brain Behav. Evol.* **62**, 201–211 (2003).
4. Y. Wang, B. J. Frost, Time to collision is signalled by neurons in the nucleus rotundus of pigeons. *Nature* **356**, 236–238 (1992).
5. W. Schiff, J. A. Caviness, J. J. Gibson, Persistent fear responses in rhesus monkeys to the optical stimulus of "looming." *Science* **136**, 982–983 (1962).
6. W. Ball, E. Tronick, Infant responses to impending collision: Optical and real. *Science* **171**, 818–820 (1971).
7. M. Yilmaz, M. Meister, Rapid innate defensive responses of mice to looming visual stimuli. *Curr. Biol.* **23**, 2011–2015 (2013).
8. F. Wang, E. Li, L. De, Q. Wu, Y. Zhang, OFF-transient alpha RGCs mediate looming triggered innate defensive response. *Curr. Biol.* **31**, 2263–2273.e3 (2021).
9. L. Huang *et al.*, A retinoraphe projection regulates serotonergic activity and looming-evoked defensive behaviour. *Nat. Commun.* **8**, 14908 (2017).
10. D. Cai, X. Luo, K. Shen, Y. Shen, GABAergic retinal ganglion cells regulate innate defensive responses. *Neuroreport* **32**, 643–649 (2021).
11. R. N. Lees, A. F. Akbar, T. C. Badea, Retinal ganglion cell defects cause decision shifts in visually evoked defense responses. *J. Neurophysiol.* **124**, 1530–1549 (2020).
12. C. Shang *et al.*, A parvalbumin-positive excitatory visual pathway to trigger fear responses in mice. *Science* **348**, 1472–1477 (2015).
13. P. Wei *et al.*, Processing of visually evoked innate fear by a non-canonical thalamic pathway. *Nat. Commun.* **6**, 6756 (2015).
14. C. Shang *et al.*, Divergent midbrain circuits orchestrate escape and freezing responses to looming stimuli in mice. *Nat. Commun.* **9**, 1232 (2018).
15. P. Dean, P. Redgrave, G. W. Westby, Event or emergency? Two response systems in the mammalian superior colliculus. *Trends Neurosci.* **12**, 137–147 (1989).
16. D. A. Evans *et al.*, A synaptic threshold mechanism for computing escape decisions. *Nature* **558**, 590–594 (2018).
17. Z. Zhou *et al.*, A VTA GABAergic neural circuit mediates visually evoked innate defensive responses. *Neuron* **103**, 473–488 e476 (2019).
18. J. Cang, E. Savier, J. Barchini, X. Liu, Visual function, organization, and development of the mouse superior colliculus. *Annu. Rev. Vis. Sci.* **4**, 239–262 (2018).
19. S. D. Gale, G. J. Murphy, Distinct representation and distribution of visual information by specific cell types in mouse superficial superior colliculus. *J. Neurosci.* **34**, 13458–13471 (2014).
20. S. D. Gale, G. J. Murphy, Active dendritic properties and local inhibitory input enable selectivity for object motion in mouse superior colliculus neurons. *J. Neurosci.* **36**, 9111–9123 (2016).
21. H. Byun *et al.*, Molecular features distinguish ten neuronal types in the mouse superficial superior colliculus. *J. Comp. Neurol.* **524**, 2300–2321 (2016).
22. C. A. Villalobos, Q. Wu, P. H. Lee, P. J. May, M. A. Basso, Parvalbumin and GABA microcircuits in the mouse superior colliculus. *Front. Neural Circuits* **12**, 35 (2018).
23. L. F. Abbott, W. G. Regehr, Synaptic computation. *Nature* **431**, 796–803 (2004).
24. B. Hutcheon, Y. Yarom, Resonance, oscillation and the intrinsic frequency preferences of neurons. *Trends Neurosci.* **23**, 216–222 (2000).
25. J. D. Victor, How the brain uses time to represent and process visual information(1). *Brain Res.* **886**, 33–46 (2000).
26. R. V. Shannon, F. G. Zeng, V. Kamath, J. Wygonski, M. Ekelid, Speech recognition with primarily temporal cues. *Science* **270**, 303–304 (1995).
27. S. Thorpe, A. Delorme, R. Van Rullen, Spike-based strategies for rapid processing. *Neural. Netw.* **14**, 715–725 (2001).
28. J. S. Dittman, A. C. Kreitzer, W. G. Regehr, Interplay between facilitation, depression, and residual calcium at three presynaptic terminals. *J. Neurosci.* **20**, 1374–1385 (2000).
29. B. A. Carlson, Temporal-pattern recognition by single neurons in a sensory pathway devoted to social communication behavior. *J. Neurosci.* **29**, 9417–9428 (2009).
30. Y. Yao *et al.*, Visual cue-discriminative dopaminergic control of visuomotor transformation and behavior selection. *Neuron* **89**, 598–612 (2016).
31. U. C. Drager, D. H. Hubel, Responses to visual stimulation and relationship between visual, auditory, and somatosensory inputs in mouse superior colliculus. *J. Neurophysiol.* **38**, 690–713 (1975).
32. G. De Franceschi, T. Vivattanasam, A. B. Saleem, S. G. Solomon, Vision guides selection of freeze or flight defense strategies in mice. *Curr. Biol.* **26**, 2150–2154 (2016).
33. T. A. Munch *et al.*, Approach sensitivity in the retina processed by a multifunctional neural circuit. *Nat. Neurosci.* **12**, 1308–1316 (2009).
34. T. Mager *et al.*, High frequency neural spiking and auditory signaling by ultrafast red-shifted optogenetics. *Nat. Commun.* **9**, 1750 (2018).
35. K. Yuge *et al.*, N-methyl-N-nitrosourea-induced photoreceptor apoptosis in the mouse retina. *In Vivo* **10**, 483–488 (1996).
36. S. Hattar, H. W. Liao, M. Takao, D. M. Berson, K. W. Yau, Melanopsin-containing retinal ganglion cells: Architecture, projections, and intrinsic photosensitivity. *Science* **295**, 1065–1070 (2002).
37. N. Y. Tsai *et al.*, Trans-Seq maps a selective mammalian retinotectal synapse instructed by nephronectin. *Nat. Neurosci.* **25**, 659–674 (2022).
38. K. Reinhard *et al.*, A projection specific logic to sampling visual inputs in mouse superior colliculus. *Elife* **8**, e50697 (2019).
39. A. A. George, A. M. Lyons-Warren, X. Ma, B. A. Carlson, A diversity of synaptic filters are created by temporal summation of excitation and inhibition. *J. Neurosci.* **31**, 14721–14734 (2011).
40. J. S. Dittman, A. C. Kreitzer, W. G. Regehr, Interplay between facilitation, depression, and residual calcium at three presynaptic terminals. *J. Neurosci.* **20**, 1374–1385 (2000).
41. G. Nagel *et al.*, Light activation of channelrhodopsin-2 in excitable cells of Caenorhabditis elegans triggers rapid behavioral responses. *Curr. Biol.* **15**, 2279–2284 (2005).
42. J. L. Hoy, H. I. Bishop, C. M. Niell, Defined cell types in superior colliculus make distinct contributions to prey capture behavior in the mouse. *Curr. Biol.* **29**, 4130–4138.e5 (2019).
43. E. A. Pnevmatikakis, A. Giovannucci, NoRMCorre: An online algorithm for piecewise rigid motion correction of calcium imaging data. *J. Neurosci. Methods* **291**, 83–94 (2017).